minerals

MDPI

Article

Ladle Steel Slag in Activated Systems for Construction Use

Diego Aponte, Oriol Soto Martín, Susana Valls del Barrio * and Marilda Barra Bizinotto

Department of Civil and Environmental Engineering, Universitat Politècnica de Catalunya (UPC-Barcelona Tech), C/Jordi Girona, 1-3, Campus Nord, Building B1. C.P., 08034 Barcelona, Spain; diego.fernando.aponte@upc.edu (D.A.); osm.oriol23@gmail.com (O.S.M.); marilda.barra@upc.edu (M.B.B.)

* Correspondence: susanna.valls@upc.edu

Received: 18 June 2020; Accepted: 29 July 2020; Published: 31 July 2020

Abstract: The construction industry needs to reduce greenhouse gases, in which cement production is currently responsible for generating between 4% and 6% of the total CO_2 released into the atmosphere. Similarly, many industries produce large amounts of solid waste, which often have low value-added applications or are directly taken to landfills, with consequent negative environmental impacts. One of these industries is the steel industry, which in 2016 generated 18.4 Mt of slag (melting and refining slag) among all European Union countries. In terms of refining steel slag (ladle or white slag), it is estimated that for each ton of steel, between 20 and 30 kg of slag is produced; that is, in 2016, more than 700,000 tons of white slag were generated. It is also known that this material has cementitious properties and can be used as a precursor in alkaline activation processes. Depending on the concentrations used of the activating agent, a higher or lower mechanical performance of the developed materials can be obtained. This work studied the alkali activation of a ladle slag used to manufacture mortars, subjecting them to an initial curing of 24 h at different temperatures (20, 40, and 70 °C). Sodium silicate and sodium hydroxide were used as activating agents, using percentages of Na_2O between 5% and 10% to obtain an optimal dosage of the activator. The physical and mechanical properties of the mortars were evaluated at different ages of curing. In addition, monitoring was undertaken of linear shrinkage due to drying and the mineralogical changes due to activation and curing time.

Keywords: ladle furnace slag; alkali-activated slag; waste; mechanical properties; shrinkage; mineralogical analysis

1. Introduction

The construction industry is one of the largest and most active sectors in Europe and globally. The production of building materials generates large amounts of CO_2 emitted into the atmosphere, in addition to large amounts of waste [1]. At present, the demand for Portland cement (an essential material in this sector) continues to increase, a situation that generates a continuous effort to find substitutes for natural materials (non-renewable), as well as for cement. This involves utilizing alternative types of cement in mortars, fillers, or concretes [2].

Different alternative materials have been used as replacements for Portland cement, and among the most common are fly ash, blast furnace slag, silica fume, and limestone filler. In recent years, the possibility of using other materials has also been studied, including steelworks refining slags (ladle furnace slag or white slag).

Steel slag is a residue from steel production, which can be either black slag (melting stage) or white slag (refining stage), depending on the stage at which it is obtained. In the European Union in 2016, 18.4 Mt of steel slag (black and white) were produced [3,4], of which it is estimated that

more than 700,000 tons were white slag because, for every ton of steel, between 20 and 30 kg of this slag is produced [3]. This material has been evaluated in different uses as a cementing agent in soil stabilization [5,6], a binder in mortars and concretes [7,8], and as a filler material for self-compacting concretes [9,10].

Alkaline activation is a field of research that has re-emerged as a viable option for obtaining cementitious materials that can replace Portland cement [11]. Activation is a chemical re-polymerization process in which a fine aluminosilicate-based material (precursor) is mixed with an alkaline agent (activator) to produce a paste capable of setting and hardening in a controllable time [11]. Good mechanical properties and high resistance to fire and acids are the most remarkable properties of these materials, but they depend on the nature of the precursor and the quantities of the activator used. The reactions observed in these materials are a dissolution, transport of the compounds, and finally, a re-polymerization [12,13]. The re-polymerization produces rigid chains that can be in the range of amorphous to semi-crystalline materials. The final product will depend on the amount of calcium in the system and can be sodium silicate hydrate with aluminum (N-A-S-H type), with low calcium content, or calcium silicate hydrate with aluminum (C-A-S-H type), with high calcium content [14–16]. Therefore, it is of great interest in the context of alternative binders, which may be environmentally friendly, to understand their possible applications, in addition to the evolution of their properties. Unfortunately, there are limited studies in the technical literature that have produced activated materials exclusively based on ladle furnace slag. Generally, refining slag is used in combination with other materials such as blast furnace slag, fly ash, or metakaolin.

Salman et al. [17] proposed that refining slag can be activated, but its reaction will depend on the mineralogical composition and the fineness of the material. The high calcium content and crystallinity of the slag can be a problem because the most reactive phase is expected to be the amorphous phase. In this work it was found that activation with 5 M NaOH and Na-Silicate followed by steam curing at 80 °C produces mortars with a compressive strength of 40 MPa at 90 days. The results also show that the higher the quantity of silicates in the mixture, the higher the strength.

In the same vein, Murri et al. [18] observed that the crystalline phases and the Ca content influence the final composition of the activated material, finding that at high liquid/solid ratios the formation of the CASH phase is favored. Chien et al. [19] produced activated slag pastes using a SiO_2/Na_2O molar ratio equal to 1, varying the alkaline agent content from 4% to 8%. It was observed that as the amount of Na_2O in the system increases, the mechanical properties of the material increase, but the shrinkage also increases significantly. It has also been shown that increasing the L/S ratio dilutes the ion concentration in the matrix which can affect the structure of the activated material and its shrinkage.

Rivera et al. [20] studied activated materials using fly ash and refining slag, showing that the incorporation of the slag into the system results in a decrease in mechanical properties. The study noted that the high content of Ca in the slag increases the structural complexity of the matrix formed from the activation, associated with the formation of the CASH gel. Finally, it was concluded that in the fly ash and slag mixtures, at 28 days, the SiO_2/Al_2O_3 ratio and the interaction of the variables SiO_2/Al_2O_3 and Na_2O/SiO_2 are not statistically significant, possibly due to the greater influence of the CaO/SiO_2 variable.

Finally, relevant results, but in contrast to other works, are those shown by Xu et al. [21], which indicated that NaOH, Na_2SO_4, and Na_2SiO_3, in concentrations of 1 M, 2 M and 4 M, are not effective activators for the refining slag, with the best compressive strength obtained with waterglass (<2 MPa at 28 days). The mechanical results obtained are similar when using NaOH and Na_2SO_4 (<1 MPa). It is possible that the low values obtained are due to a high particle size (<300 μm), so ground granulated blastfurnace slag (GGBS) is added to improve the compressive strength.

The current research aims to study the possibility of obtaining a binder by alkaline activation from ladle furnace slag (white slag) and to evaluate its application to obtaining mortars that can be used in construction. The effect of the curing temperature on the physical–mechanical properties of the

mortars, and on their shrinkage, was also studied. Finally, changes in the matrix were analyzed from a mineralogical point of view.

2. Materials and Experimental Methods

2.1. Materials

In this work, ladle furnace slag (white slag) from a carbon steel factory located in Spain was used. In the steel plant, the slag was subjected to primary cooling with water to reduce the temperature and facilitate its handling. It was then taken to a recovery plant where its steel content was removed and screened to obtain a material with a particle size of 0–25 mm. This material was stored for three months to weather it and minimize expansion problems. A 0–25 mm slag sample was taken and, following the UNE EN 932-2 standard, a representative sample was obtained, from which a 0–0.063 mm fraction was used as the study material.

Limestone sand was used as fine aggregate (0–5 mm), distilled water and reagents (activating agents) of sodium silicate (waterglass) and sodium hydroxide, both from PanReac AppliedChem brand. The waterglass was composed of 22.99% SiO_2, 7.01% Na_2O, and 70% water (quantities by weight).

For the chemical characterization, this study employed the X-Ray Fluorescence (XRF) technique, using the Panalytical model PW2400 Spectrometer (Malvern Panalytical, Malvern, UK). The mineralogical characterization of the slag and reaction compounds were performed using the X-Ray Diffraction technique (XRD) using a Bruker D8-A25 powder Diffractometer (Bruker Corporation, Billerica, MA, USA), with KαCu radiation (λ= 1.5418 Å), graphite monochromator and scintillation detector, under X-ray tube conditions of 30 mA and 40 kV. The angular speed was 0.05 (2θ) every 3 s, with a scanning range of 2θ between 5° and 60°. The results of the chemical composition are shown in Table 1, while the crystalline compounds determined can be seen in Table 2 and Figure 1.

Table 1. Chemical composition of ladle slag (XRF).

Element	Quantity (%)	Element	Quantity (%)
CaO	52.76	TiO_2	0.33
SiO_2	21.58	Cr_2O_3	0.08
MgO	5.86	K_2O	0.05
Al_2O_3	5.07	ZnO	0.04
Fe_2O_3	2.37	P_2O_5	0.03
SO_3	1.37	Others	1.74
MnO	0.91	LOI *	7.81

* LOI: Loss on Ignition.

Table 2. Mineral composition of ladle slag (XRD).

Id.	Mineral	Chemical Formula
1	Calcium silicate	β-C_2S
2	Portlandite	$Ca(OH)_2$
3	Periclase	MgO
4	Brucite	$Mg(OH)_2$
5	Gehlenite	$Ca_2Al_2SiO_7$
6	Calcite	$CaCO_3$
7	Magnesian calcite	$(Ca,Mg)CO_3$
8	Mayenite	$Ca_{12}Al_{14}O_{33}$
9	Merwinite	$Ca_3Mg(SiO_4)_2$

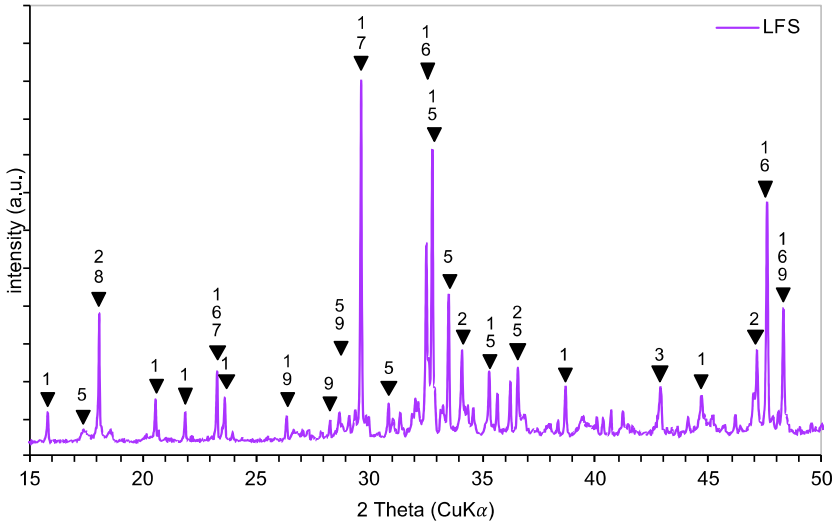

Figure 1. XRD pattern of ladle furnace slag (LFS).

The white slag studied was mainly composed of calcium and silicon, with smaller amounts of magnesium and aluminum. The presence of iron was observed, which may be due to contamination with black slag or remaining steel. The CaO/SiO_2 ratio was 2.44, while the Al_2O_3/SiO_2 ratio was 0.23 and the basicity index $(CaO + MgO)/(SiO_2 + Al_2O_3)$ was 2.20. The XRD of the white slag showed a complex material in mineralogical terms. Figure 1 shows the presence of an amorphous phase and the presence of crystalline compounds such as calcium silicates, calcium carbonates, calcium silico-aluminates, calcium aluminates, portlandite, and periclase. An important aspect to consider is the presence of periclase (MgO), which, when hydrated and producing brucite ($Mg(OH)_2$), generates an increase in its volume which is translated into internal tensions within the matrix and observed as fissures and cracks in the material containing it.

2.2. Manufacturing Alkali-Activated Mortar Specimen

Initially, four types of pastes (I–IV) were produced with a Si/Na ratio of 1.2 and 2, a liquid/solid ratio of 0.35, and a sodium percentage of 5% and 10% of the total weight slag (Table 3). The above values were taken from other works [11,15,18,22]. NaOH content in the mixture varied from 2% to more than 12%, while the Si/Na ratio ranged from 0.2 to 4. The mixing procedure followed was the one set out in the UNE EN 196-3 standard. The above pastes were used to define the variables of Si/Na ratio and % of Na_2O in correspondence to the setting time and initial hardness in a qualitative manner. From the initial observations, it was found that: type I paste presented a very fluid consistency, and after 24 h of manufacture it had not entirely hardened; type II paste presented a swift setting time of fewer than 15 min; type III paste presented a setting time of more than 40 min, and after 24 h it had partially hardened; type IV paste presented a very fluid consistency, and after 15 min it had begun to set. With these results, a new dosage (V) was made, with a Si/Na ratio of 1.2% and 7% Na_2O, obtaining good characteristics resistant to 24 h with an initial setting time of 30 min. The liquid/solid ratio was calculated considering the amount of water in the waterglass plus additional water to obtain a specific value (0.35 or 0.45), while the solid part was assumed to be the amount of slag plus the solids in the waterglass and the sodium hydroxide.

Table 3. Dosage of the pastes to define the activation parameters.

Type	Ms (Si/Na)	%Na_2O	Ladle Slag (g)	Na_2SiO_3 (g)	NaOH (g)	H_2O (g)	L/S Ratio
I	1.2	5	150	33.38	6.26	58.20	0.35
II	2			63.135	3.98	60.50	0.35
III	1.2	10		83.25	12.51	65.60	0.35
IV	2			126.27	7.94	88.00	0.45
V	1.2	7	100	35.4	5.8	40.70	0.35

With the V dosage of the pastes, the mortars were manufactured and cured for the first 24 h at three different temperatures (20, 40, and 70 °C), which were named accordingly (M20, M40, and M70). Mortars cured at 40 and 70 °C after molding were covered with plastic film to avoid water loss and allow reactions. Mortars that did not have a good seal were observed to have surface cracking and were therefore not used in the tests. However, the presence of micro-cracks cannot be discarded and could influence the results obtained. The subsequent curing was carried out in a humid chamber at 20 °C and 95% relative humidity (R.H.), until the respective test date. In the dosage of the mortars, the Si/Na ratio (1.2) and the percentage of Na_2O (7%) were maintained, but the liquid/solid ratio was increased to 0.55 to obtain a good consistency for the compaction of the material. The mixing and compacting procedure used in the manufacture of mortars was that specified in the UNE EN 196-1 standard. The dosage of the mortars is shown in Table 4.

Table 4. Dosage of mortars studied.

Material	Quantity
Si/Na	1.2 g
Na_2O	7%
Ratio L/S	0.55 g
Ladle slag	450 g
Sodium Silicate	159.1 g
Sodium hydroxide	26.3 g
Water	176.9 g
Sand	1350 g

Finally, activated paste specimens (without sand) were manufactured and subjected to the same curing processes as the mortars. These samples were used to determine the mineralogical changes due to the alkali activation process, temperature, and curing time.

2.3. Tests Performed

Physical–mechanical properties were determined at the ages of 7, 28, and 56 days of curing. The results presented are the average of three samples that were made in 4 × 4 × 16 cm molds according to the UNE EN 196-1 standard.

At each age of test, the physical properties determined were the density, absorption, and porosity of the mortars, following the ASTM C642 standard. The mechanical properties determined were the flexural strength and the compressive strength, under the guidelines of the UNE EN 196-1 standard. Concerning the shrinkage processes of the different samples, the tests were based on the ASTM C596 and ASTM C490 standards. For the shrinkage tests, 25 × 25 × 260 mm mortar samples were used, which were cured in the same way as the rest of the mortars, but after seven days of curing in a humid chamber, they were removed and left in an environment at 22 °C and 55% relative humidity to carry out the longitudinal change measurements. Simultaneously, the weight change measurements were made.

To evaluate the mineralogical changes in the activated pastes, the alcohol-acetone method was used to stop the hydration processes at each curing age. This procedure was performed as follows:

initially a sample of 10 g of paste was taken and immersed in alcohol for a period of 4 h. The sample was then milled in an agate mortar until all particles passed through a 0.063 mm sieve. Finally, the powdered sample was placed on a paper filter and the acetone was passed through it until the sample was completely dry, and an X-ray diffraction test was performed. The identification of all phases was carried out with Bruker's Diffract EVA software with PDF-2 database.

3. Results

3.1. Density, Absorption, and Porosity of the Activated Mortars

The results of the physical properties of the different mortars at different ages are shown in Figure 2. It can be seen that the density of all the mortars increases with the curing time. M20 and M70 mortars have similar densities at all ages, while M40 mortar has a lower density.

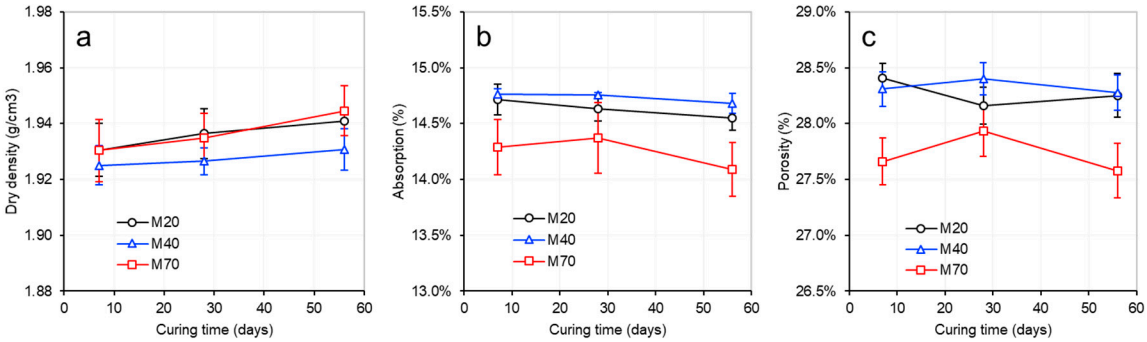

Figure 2. Physical properties of the different mortars. (**a**) Dry density, (**b**) absorption, and (**c**) porosity.

The absorption and porosity of the different mortars show a decrease with the curing time; however, this reduction is small and, in the case of the M40 mortar, it can be said that there are no significant changes. Mortars cured at 70 °C have the lowest absorption and porosity, but the values of all mortars are in the range of 14% to 15% for absorption and 27.5% to 28.5% for porosity.

3.2. Mechanical Properties of the Activated Mortars

The results of the flexural test and subsequent compression test are shown in Figure 3. In all cases, the mechanical performance increases with the curing time of the mortars. M20 and M40 mortars show similar values of flexural and compressive strength at different test ages, and M70 mortar shows the best performance in both flexural and compressive strength.

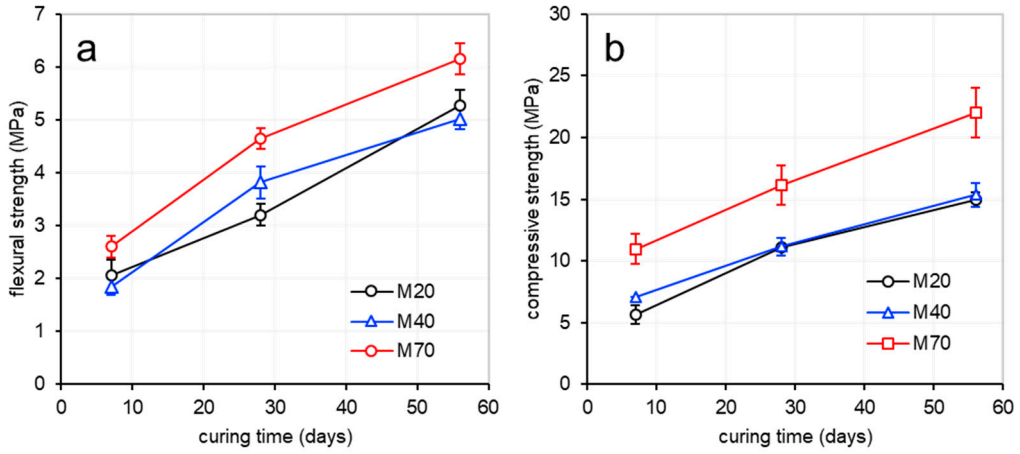

Figure 3. Mechanical properties of activated mortars. (**a**) Flexural strength, and (**b**) compressive strength.

The increase in mechanical properties with the curing time is remarkable for all mortars. The average increase in flexural strength, from 7 to 55 days, for all mortars is 155%, and in the case of compressive strength, it is 127%. Mortars cured at 70 °C have higher flexural (29%) and compressive (55%) strengths than mortars cured at 20 and 40 °C. As is known, the effect of the curing temperature of the activated materials plays a fundamental role in accelerating the speed of polymerization of the material.

3.3. Linear Retraction and Weight Loss by Drying

Alkaline-activated materials are known to have a higher shrinkage than cement-based materials, leading to durability problems. In this regard, Palacios et al. [22] have shown that the drying shrinkage of activated materials can be up to four times that of Portland cement-based materials. Similar results have been shown by Shi et al. [23], who mention that activated concretes have significantly higher shrinkage than conventional concrete. The high shrinkage of activated materials is attributed to higher chemical shrinkage, a higher degree of saturation, and lower material stiffness [24,25].

Figure 4 shows the longitudinal change and weight change behavior of activated and cured mortars at different temperatures. During the first seven days of wet curing (20 °C and 95% R.H.), the mortar bars show a weight gain (<1%) and a slight expansion, which can be considered negligible (<0.05%). The above behavior is consistent with the results obtained by Cartwright et al. [24].

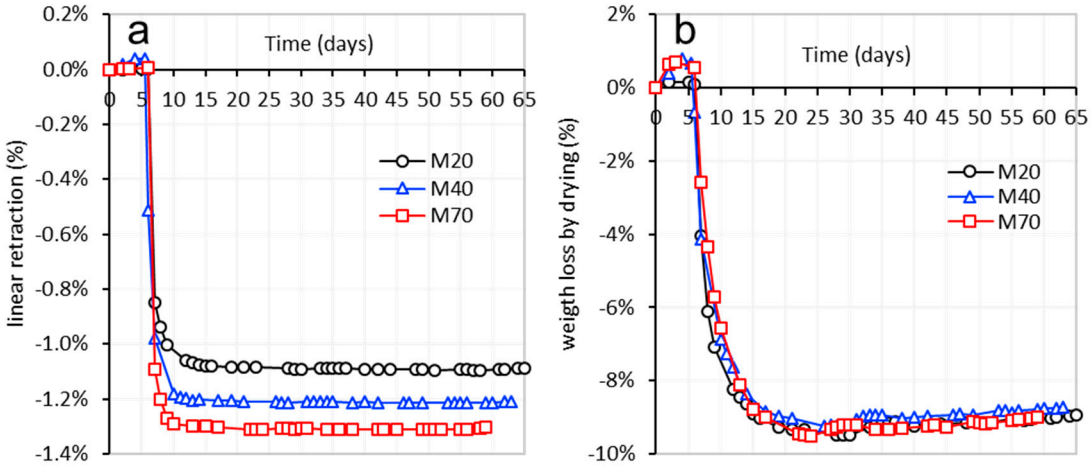

Figure 4. Shrinkage and weight loss over time in all types of activated mortars. (**a**) Linear retraction, and (**b**) weight loss.

At the beginning of the drying process, all mortars show a significant shrinkage; 90% of the total shrinkage, in all cases, originates in the first three days of drying, and is higher in the mortars that cure at higher temperatures. Compared to the initial cure at 20 °C, applying a cure at 40 °C generates an increase of 11.5% of shrinkage, and 20.5% if the cure is performed at 70 °C. Figure 4 also shows the loss of mass by drying of all mortars. In all cases, the curves are similar, and the mass loss values at the end of 60 days are approximately 9%, with a mass loss of more than 6% in the first three days of drying.

Figure 5 shows the behavior of weight loss versus linear shrinkage by drying. It can be seen that the same weight loss generates more significant shrinkage in mortars that cure initially at higher temperatures. For example, if mortars are subjected to a 2% water loss, the shrinkage of the M20 is 0.41%, M40 is 0.7%, and M70 is 0.9%—more than twice that of the mortar cured at 20 °C.

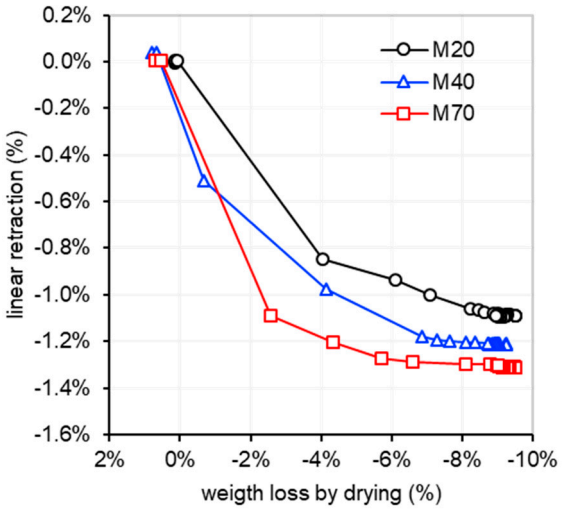

Figure 5. Shrinkage vs. weight loss for activated mortars.

The shrinkage process in activated materials is not fully understood, however, Zhenming et al., [26] states that this phenomenon is due to two mechanisms: self-desiccation and a reduction of steric-hydration forces due to the consumption of ions in the activation process. The above approach is related to the results obtained because, in mortars cured at 70 °C, the reaction of compounds is accelerated, generating greater shrinkage (higher consumption of ions) than those cured at 40 and 20 °C. It should also be considered that the higher the curing temperature, the more refined the pores, producing greater pressure within them and, therefore, greater shrinkage, despite having the same weight loss as mortar cured at lower temperatures.

3.4. Mineralogical Changes Observed in Activated Mortars

As mentioned above, white slag is a mineralogically complex material, presenting crystalline mineral phases with some material in amorphous form. Therefore, the most remarkable aspect is that the differently activated pastes present a higher proportion of amorphous material, which can be observed between 26° and 37° 2θ compared to the raw slag (Figure 6). It should also be mentioned that the peaks of the crystalline phases become broader and less defined. The increase of the amorphous material is due to the reaction of some compounds of the slag, as well as the process of dissolution and polymerization of the compounds due to the activation, generating compounds of the type C(N)ASH.

The alkaline activation process also generates the disappearance or reduction in the intensity of some phases such as portlandite, mayenite, and beta-calcium silicate. A reduction in the intensity of the peak relative to periclase can also be observed. The appearance of new phases such as calcite ($CaCO_3$), katoite ($Ca_3Al_2(SiO_4)1.5(OH)_6$), and hydrocalcite ($Mg_6Al_2(CO_3)(OH)_{16}{\cdot}4(H_2O)$) is evident. The katoite belongs to the garnet family, with a formula of the type $X_3Y_2(SiO_4)_3$, where the X site is occupied by Ca^{2+}, Mg^{2+}, and Fe^{2+}, while the Y site is occupied by Al^{3+} or Fe^{3+}. In the case of hydrated granules, $[SiO_4]^{4-}$ is partially replaced by OH^- [27]. Hydrocalcite is a compound with a formula of the type $Mx_2{+}My_3{+}(OH)_{2x+3y}$-$nz(An\text{-})^{z-}{\cdot}mH_2O$, where An- can be Cl^-, CO_2^{3-}, or NO_3^-. Mg^{2+} and Al^{3+} have been identified in materials-activated alkali with raw materials containing more than 5% MgO [28,29].

Figure 7 shows important changes observed in the range 29° to 35° 2θ. The first is the appearance of the peak relative to calcite ($CaCO_3$) and a decrease in the peak relative to beta-calcium silicate and magnesian calcite. This change may be due to the conversion of portlandite into carbonate by a carbonation process, as well as the influence of the alkaline activation process. The disappearance of the portlandite-related peak and a decrease in the mayenite peak's intensity are also observed. Beta- calcium silicate peaks have also suffered a decrease in intensity and an increase in peak width, which may be related to their possible reaction to generate hydrated compounds. Finally, we observe

the appearance of the peak relative to brucite ($Mg(OH)_2$), which is the hydration product of periclase and can be accelerated by being in a highly alkaline medium.

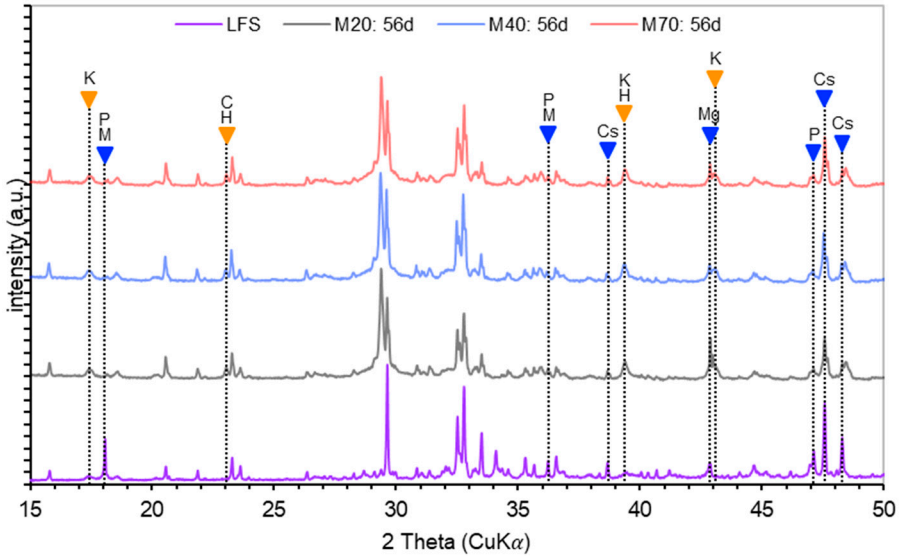

Figure 6. XRD patterns of raw slag and alkali-activated slag at different temperatures and 56 days of curing. K: katoite, P: portlandite, M: mayenite, C: calcite, H: hydrocalcite, Cs: calcium silicate, Mg: periclase.

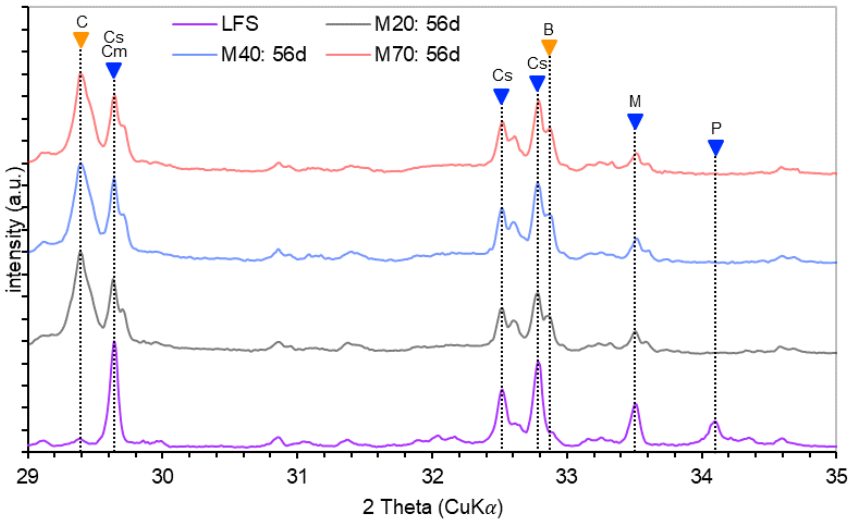

Figure 7. Detail of the changes between 29° and 34° 2θ between the raw slag and the activated slag at different temperatures and 56 days of curing C: calcite, Cs: calcium silicate, Cm: magnesian calcite, B: brucite, M: mayenite, P: portlandite.

Figures 8–10 show the mineralogical changes (XRD) at different curing ages for the pastes cured at 20, 40, and 70 °C respectively. At the different ages, there are no significant changes in the compounds formed, and an increase in the amorphous fraction of the pastes can be observed, which is higher in pastes cured at higher temperatures.

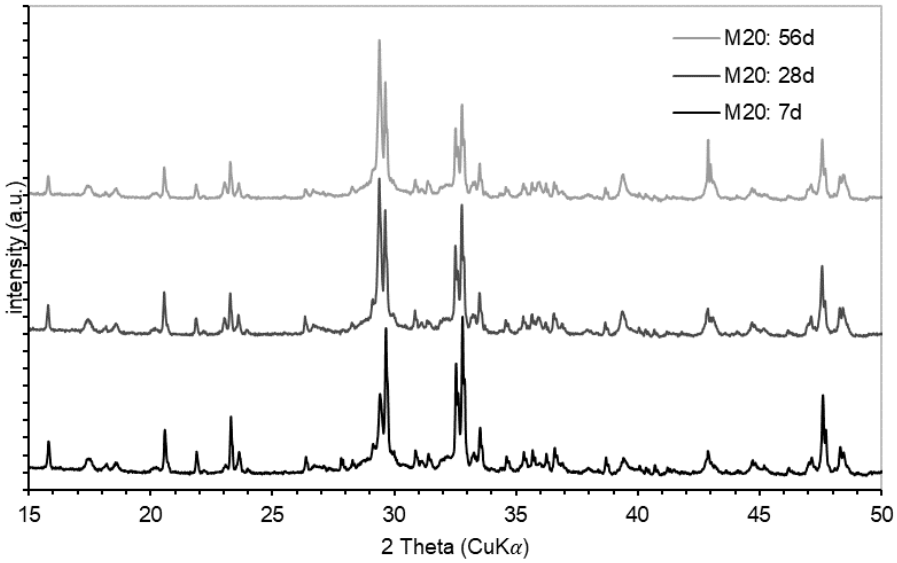

Figure 8. XRD patterns of alkali-activated slag at 20 °C and different curing times.

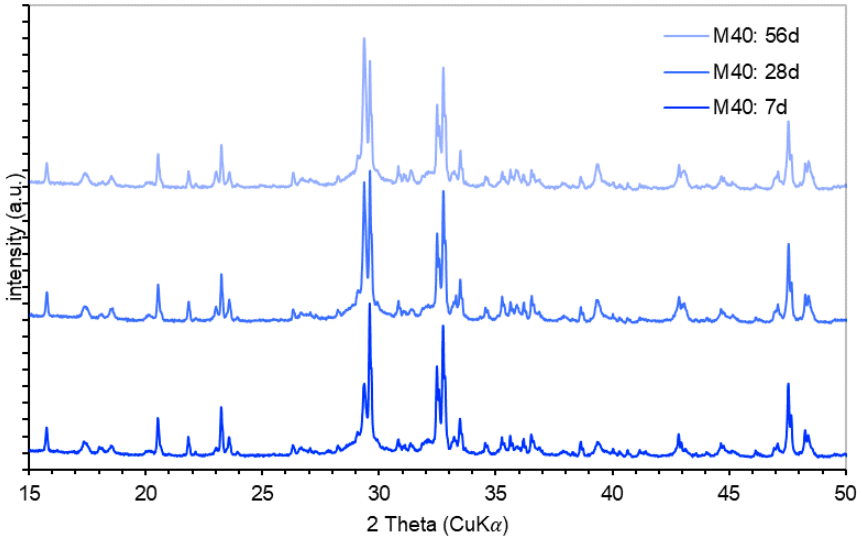

Figure 9. XRD patterns of alkali-activated slag at 40 °C and different curing times.

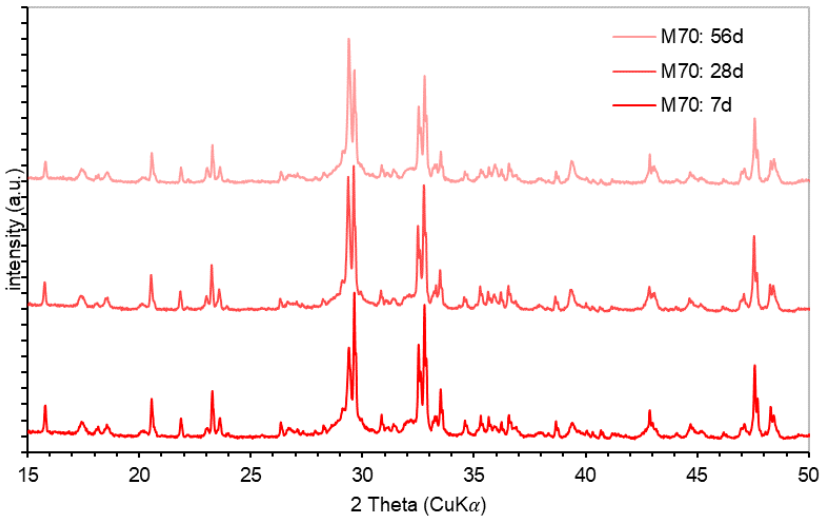

Figure 10. XRD patterns of alkali-activated slag at 70 °C and different curing times.

4. Conclusions

In this work, the possibility of using ladle slag as a precursor in obtaining an alkaline-activated mortar was investigated. The effect of the initial curing temperature on the physical and mechanical properties and the mineralogical changes of the materials produced was considered. It can be concluded that:

- The difference in dry density between the mortars is low, reaching the highest difference at 56 days of cure between mortars cured at 40 and 70 °C.
- Absorption and porosity are similar at all curing ages, for mortars cured at 20 and 40 °C, while mortars cured at 70 °C show lower values in these two properties.
- Shrinkage by drying was more significant, the higher the initial curing temperature of the mortars, with the greatest shrinkage generated in the first days of drying. The weight loss by drying was the same in all mortars. The difference in shrinkage may be due to different pore size distributions, with greater pore refinement being obtained at higher curing temperatures, which will generate greater shrinkage.
- Promising values were obtained in terms of mechanical properties. The compressive strength of mortars cured at 20 and 40 °C, after 56 days of curing, reaches 15 MPa, but increases to 22 MPa for mortars cured at 70 °C.
- The evolution of the mineralogical composition showed the formation of new compounds (magnesian calcite, brucite, katoite, and hydrocalcite), and the disappearance of others (portlandite, mayenite, and periclase) in the activation process, as well as the increase of the amorphous phase.

Author Contributions: Conceptualization: D.A., S.V.d.B., and M.B.B.; Methodology: D.A., and O.S.M.; Validation and supervision: D.A., S.V.d.B., and M.B.B.; Investigation: D.A., S.V.d.B., and M.B.B.; Resources: O.S.M., and D.A., Original draft preparation: S.V.d.B., and D.A.; Writing-review and editing: D.A.; Visualization: D.A., and S.V.M.; Supervison: D.A., and M.B.B.; Project administration: M.B.B. All authors have read and agreed to the published version of the manuscript.

Funding: This research received no external funding.

Conflicts of Interest: The authors declare no conflict of interest.

References

1. Anink, D.; Boonstra, C.; Mak, J. *Handbook of Sustainable Building. An Environmental Preference Method for Selection of Materials for Use in Construction and Refurbishment*; James & James (Science Publishers) Limited: London, UK, 1996.
2. Motorwala, A.; Shah, V.; Kammula, R.; Nannapaneni, P.; Raijiwala, D.B. Alkali activated fly-ash based geopolymer concrete. *Int. J. Emerg. Technol. Adv. Eng.* **2013**, *3*, 159–166.
3. UNESID. Unión de Empresas Siderúrgicas. Available online: https://unesid.org/el-sector-el-sector-en-2016-producciones-basicas.php (accessed on 16 January 2020).
4. Euroslag. Available online: https://www.euroslag.com/products/statistics/statistics-2016/ (accessed on 10 December 2019).
5. Manso, J.M.; Losañez, M.; Polanco, J.A.; González, J. Ladle furnace slag in construction. *J. Mater. Civ. Eng.* **2005**, *17*, 513–518. [CrossRef]
6. Ortega-López, V.; Manso, J.M.; Cuesta, I.I.; González, J. The long term accelerated expansion of various ladle furnace basic slag and their soil stabilization applications. *Constr. Build. Mater.* **2014**, *68*, 455–464. [CrossRef]
7. Adolfsson, D.; Engström, F.; Robinson, R.; Björkman, B. Cementitious phases in ladle slag. *Steel Res. J.* **2011**, *82*, 398–403. [CrossRef]
8. Herrero, T.; Vegas, I.; Santamaria, A.; San-Jose, J.T.; Skaf, M. Effect of high alumina ladle furnace slag as cement susbtitution in masonry mortars. *Constr. Build. Mater.* **2016**, *123*, 404–413. [CrossRef]
9. Anastasiou, E.K.; Papayianni, I.; Papachristoforou, M. Behavior of self compacting concrete containing ladle furnace slag and steel fiber reinforcement. *Mater. Des.* **2014**, *59*, 454–460. [CrossRef]

10. Sideris, K.K.; Tassos, C.; Chatzopoulos, A.; Manita, P. Mechanical characteristics and durability of self compacting concretes produced with ladle furnace slag. *Constr. Build. Mater.* **2018**, *170*, 660–667. [CrossRef]
11. Pacheco-Torgal, F.; Labrincha, J.A.; Leonelli, C.; Palomo, A.; Chindaprasit, P. *Handbook of Alkali-Activated Cements, Mortars and Concretes*; Woodhead Publishing Series in Civil and Structural Engineering; Woodhead Publishing: Sawston, UK; Cambridge, UK, 2014.
12. Komnitsas, K.; Zaharaki, D. Geopolymerisation: A review and prospects for the minerals industry. *Min. Eng.* **2007**, *20*, 1261–1277. [CrossRef]
13. Mejía, J.M.; Mejía de Gutiérrez, R.; Puertas, F. Ceniza de cascarilla de arroz como fuente de sílice en sistemas cementicios de ceniza volante y escoria activados alcalinamente. *Mater. Constr.* **2013**, *63*, 361–375. [CrossRef]
14. García-Lodeiro, I.; Fernández-Jiménez, A.; Palomo, A.; Macphee, D.E. Effect of Calcium Additions on N–A–S–H Cementitious Gels. *J. Am. Ceram. Soc.* **2010**, *93*, 1934–1940. [CrossRef]
15. Bernal, S.A.; Mejía de Gutiérrez, R.; Ruiz, F.; Quiñones, H.; Provis, J.L. High-temperature performance of mortars and concretes based on alkali-activated slag/metakaolin blends. *Mater. Constr.* **2012**, *62*, 471–488. [CrossRef]
16. Puertas, F.; Palacios, M.; Manzano, H.; Dolado, J.S.; Rico, A.; Rodríguez, J. A model for the C-A-S-H gel formed in alkali-activated slag cements. *J. Eur. Ceram. Soc.* **2011**, *31*, 2043–2056. [CrossRef]
17. Salman, M.; Cizer, Ö.; Pontikes, Y.; Snellings, R.; Vandewalle, L.; Blanpain, B.; van Balen, K. Cementitious binders from activated stainless steel refining slag and the effect of alkali solutions. *J. Hazard. Mater.* **2015**, *286*, 211–219. [CrossRef]
18. Murri, A.N.; Rickard, W.D.A.; Bignozzi, M.C.; van Riessen, A. High temperature behaviour of ambient cured alkali-activated materials based on ladle slag. *Cem. Concr. Res.* **2013**, *43*, 51–61. [CrossRef]
19. Wang, W.-C.; Wang, H.-Y.; Tsai, H.-C. Study on engineering properties of alkali-activated ladle furnace slag geopolymer. *Constr. Build. Mater.* **2016**, *123*, 800–805. [CrossRef]
20. Rivera, J.F.; Cristelo, N.; Fernández-Jiménez, A.; de Gutiérrez, R.M. Synthesis of alkaline cements based on fly ash and metallurgic slag: Optimization of the SiO_2/Al_2O_3 and Na_2O/SiO_2 molar ratios using the response surface methodology. *Constr. Build. Mater.* **2019**, *213*, 424–433. [CrossRef]
21. Bo, X.; Yi, Y. Use of ladle furnace slag containing heavy metals as a binding material in civil engineering. *Sci. Total Environ.* **2019**, *705*, 135854.
22. Palacios, M.; Puertas, F. Effect of shrinkage-reducing admixtures on the properties of alkali-activated slag mortars and pastes. *Cem. Concr. Res.* **2007**, *37*, 691–702. [CrossRef]
23. Shi, C.; Krivenko, P.; Roy, D. *Alkali-Activated Cements and Concrete*; Taylor & Francis: New York, NY, USA, 2006.
24. Christopher, C.; Farshad, R.; Aleksandra, R. Shrinkage Characteristics of Alkali-Activated Slag Cements. *J. Mater. Civ. Eng.* **2014**, *27*, B4014007.
25. Collins, F.; Sanjayan, J.G. Effect of pore size distribution on drying shrinkage of alkali-activated slag concrete. *Cem. Concr. Res.* **2000**, *30*, 1401–1406. [CrossRef]
26. Li, Z.; Lu, T.; Liang, X.; Dong, H.; Ye, G. Mechanisms of autogenous shrinkage of alkali-activated slag and fly ash pastes. *Cem. Concr. Res.* **2020**, *135*, 106107. [CrossRef]
27. Dilnesa, B.Z.; Lothenbach, B.; Renaudin, G.; Wichser, A.; Kulik, D. Synthesis and characterization of hydrogarnet $Ca_3(Al_xFe_{1-x})_2(SiO_4)_y(OH)_{4(3-y)}$. *Cem. Concr. Res.* **2014**, *59*, 96–111. [CrossRef]
28. Ke, X.; Bernal, S.A.; Provis, J.L. Controlling the reaction kinetics of sodium carbonate-activated slag cements using calcined layered double hydroxides. *Cem. Concr. Res.* **2016**, *81*, 24–37. [CrossRef]
29. Wang, S.-D.; Scrivener, K.L. Hydration products of alkali activated slag cement. *Cem. Concr. Res.* **1995**, *25*, 561–571. [CrossRef]